Journal of Metastable and Nanocrystalline Materials Vols. 20-21 (2004) pp. 617-622
online at http://www.scientific.net

Structural and Magnetic Properties of Bottom-up Synthesized $ZnFe_2O_4$ Nanoparticles

J.A. Gomes[1,a], M.H. Sousa[2,b], F.A. Tourinho[2,c]
J. Mestnik-Filho[3,d], R. Itri[4,e] and J. Depeyrot[1,f]

[1]Instituto de Física, Universidade de Brasília, C.P. 04455, 70919-970, Brasília, Brazil
[2]Instituto de Química, Universidade de Brasília, C.P. 04478, 70919-970, Brasília, Brazil
[3]Instituto de Pesquisas Energéticas e Nucleares, C.P. 11049, 05422-970, São Paulo, Brazil
[4]Instituto de Física, Universidade de São Paulo, C.P. 66318, 05315-970, São Paulo, Brazil

[a]juliano@fis.unb.br, [b]fralda@unb.br, [c]tourinho@fis.unb.br,
[d]jmestnik@baitaca.ipen.br, [e]itri@if.usp.br, [f]depeyrot@fis.unb.br

Keywords: Cation Distribution, Ferrite, Magnetic Nanoparticles, Rietveld Refinement

Abstract. Zinc ferrite nanoparticles are bottom-up synthesized and then peptized in aqueous media resulting in stable magnetic fluids. X-ray powder patterns are analyzed using Rietveld structure refinement and indicate the existence of cation inversion at the sites of the spinel-type nanocrystal. Magnetic and magneto-optical properties therefore arise and are investigated by static measurements performed on individual particles solutions.

Introduction

Magnetic properties of nanosized ferrite particles are a subject of great interest due in part to their use in high-density information storage but also in biological applications. When the nanoferrites are dispersed in a carrier liquid, the resulting colloidal suspension is called ferrofluid or magnetic fluid. These materials give risen to numerous technological applications due in part to the versatility of molecular carrier liquids such as polar and non-polar media [1]. However, such applications are dependent on the structural and magnetic properties of the nanocrystals that generally differ from those of bulk materials [2].

Spinel-type crystals present the same crystalline structure as the mineral spinel $MgAl_2O_4$, crystallizing in a close packed fcc lattice with eight formula units in the cubic unit cell, belonging to the space group $Fd3m$ (O_h^7). Spinel ferrites have the general molecular formula $(M^{2+})[Fe_2^{3+}]\,O_4^{2-}$ where M^{2+} and Fe^{3+} are the divalent and trivalent cations occupying tetrahedral (A) and octahedral (B) interstitial positions of the fcc lattice formed by O^{2-} ions. Nevertheless, a whole range of cations distribution is possible in spinels and they are better represented by the more precise formula $(M^{2+})_{(1-x)}(Fe^{3+})_x[(M^{2+})_x(Fe^{3+})_{(2-x)}]O_4$, where the ions inside the brackets are said to occupy B sites and the ions outside the bracket occupy A sites [3]. Then, x represents the so-called degree of inversion also defined as the fraction of A sites occupied by Fe^{3+} cations.

Ideal zinc ferrite ($ZnFe_2O_4$) is a normal spinel ($x = 0$) where zinc cations occupy all of the tetrahedral sites and iron ions are on the octahedral sites. Bulk material presents an antiferromagnetic ordering below 10 K [4]. However, it has been reported for $ZnFe_2O_4$ nanomaterial the existence of a significant magnetic moment, even at room temperature [5-7], as well as an increase in the ordering temperature [5]. Such effects have been associated to the presence of Fe^{3+} ions at tetrahedral sites and the consequent existence of non zero exchange interactions between iron cations on different sites [6]. This process of partial inversion is strongly dependent on the method used to prepare $ZnFe_2O_4$ nanostructured materials [7, 8], although it seems possible to make the following observations. Methods which use high temperature treatment generally lead to the

ideal normal spinel structure whereas high energy ball milling [8, 9] and soft chemical routes, such hydrothermal co-precipitation [5, 7] or reverse micelle synthesis [10], induce a certain inversion degree. Moreover, at room temperature, the saturation magnetization of zinc ferrite nanoparticles obtained by co-precipitation is found to increase with decreasing size suggesting that cation substitution is more pronounced for smaller particles [5].

In such a context, we report here on chemically synthesized magnetic fluids based on zinc ferrite nanoparticles which could be used for biological purposes due to their low iron content [7]. The chemical composition of the nanomaterial is monitored during all the synthesis process by usual chemical analysis. The cation distribution of the $ZnFe_2O_4$ nanograins is investigated using Rietveld structure refinement of x-ray powder diffractogram. Then, room temperature magnetization and magneto-optical measurements performed on colloidal solution are presented and discussed.

Experimental procedure

Samples preparation and synthesis characterization: The ferrofluid was prepared according to the procedure previously described [7]. Firstly, the ferrite nanoparticle synthesis was carried out using a hydrothermal coprecipitation aqueous solution of a $ZnCl_2$ - $FeCl_3$ mixture in alkaline medium. Then, the particles were conveniently peptized in an acidic medium by ionic strength adjustment, resulting in a stable sol of high quality. Two set of samples were prepared, named A and B, with distinct mean sizes by changing the reagents stirring speed in the synthesis environment during the coprecipitation process.

In order to obtain a maximum magnetization yield of the synthesized material, we determined the best starting metal ratio for the synthesis and the final particle stoichiometry. The chemical composition of the samples was monitored by usual chemical analysis. The magnetic yield was indirectly measured by means of a Gouy balance that detects the apparent mass increase (Δm) observed in the presence of an external field [7]. The magnetic yield of nanoparticles, which were coprecipitated out from a series of solutions of equal total metal concentration, is then measured as a function of the molar fraction $X_{Zn} = [Zn^{2+}]/[Zn^{2+} + Fe^{3+}]$.

Structural Characterization and Nanocrystal Size Determination: The crystalline structure and the mean size of nearly spheroidal shaped nanoparticle were determined by using X-ray diffraction experiments. These were realized on powder samples obtained after evaporation of the liquid sample. The measurements were performed by means of a X-ray diffractometer installed in a conventional Rigaku/Geigerflex generator operating at 40 kV/30 mA and the Cu-Kα radiation selected by a graphite monochromator. X-ray powder diffraction data were obtained in a 2θ scanning range from 25° to 80° with a step size of 0.05°(2θ) with 8 s counting time at each step, using divergence and receiving slits of 0.5° and a detection one of 0.15 °. The data sets were processed by the Rietveld refinement method using the GSAS program.

Magnetic and magneto-optical characterization: To characterize the ferrofluid samples the magnetization and magneto-optical birefringence field were investigated as a function of the applied magnetic field at room temperature. Ferrofluids magnetization were measured with a Squid device at 300 K. The setup and the method to measure the ferrofluid birefringence are described elsewhere [11].

Results and discussion

Samples preparation and synthesis characterization: Fig. 1 shows the normalized value of the magnetic material yield as a function of the zinc molar ratio. The magnetic material yield behavior is well reproduced by a third order polynomial function leading to a maximum magnetic material yield corresponding to a zinc molar ratio of 0.33 and hence to the stoichiometric $ZnFe_2O_4$ chemical formula. All of the synthesized ferrite nanoparticles utilized in this study perfectly matches

this chemical formula as confirmed by both the magnetic material yield and by the chemical analyses.

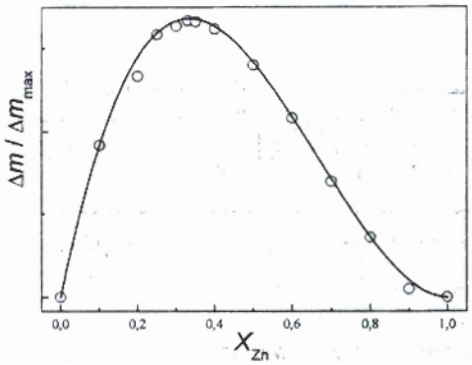

Fig. 1. Magnetic material yield as a function of the zinc molar ratio.

Structural Characterization and Nanocrystal Size Determination: The structure refinement was performed considering the *Fd3m* space group with zinc and iron atoms in the Wyckoff *8a* and *16d* special position, and O atoms in the *32e* special positions. Moreover, both octahedral and tetrahedral sites of cations and oxygen sites are assumed to be fully occupied. Then, the profile spectra was modeled using a multiterm Simpson's rule integration of the pseudo-Voigt function. Fig. 2 presents the experimental diffraction patterns, along with the calculated ones. Fig. 2 also includes the differences between them, obtained for samples A and B. As one can see, the agreement between experimental and simulated data is rather good.

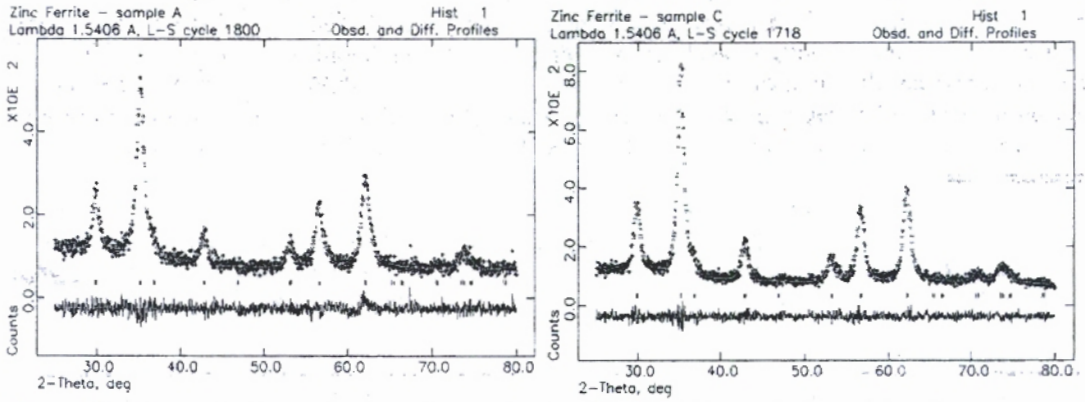

Fig. 2. Diffraction and refinement patterns for samples A and B. The difference is shown below. Plus (+) marks represent the collected data. Tic marks show the positions for the allowed reflections.

The crystallographic parameters that are refined here are a scale factor; the lattice parameter *a*, the oxygen positional parameter *u* and the inversion degree *x*. The results of the refinements are listed in Tables 1 and 2. The values of the lattice parameter, particle size and oxygen positional parameter are presented in Table 1. Moreover, the fitting quality to the experimental data can be checked by using different parameters. They are: the Gof (goodness of fit) that must tend to 1 and two reliability factors R_p and R_{wp} (two kinds of weighted differences between measured and calculated values) that must be close to or less than 10% [12, 13]. Their values are also included in Table 1. Table 2 gives the positions of the metal ions and their respective occupation fractions in each site.

Table 1: Samples structural parameters.

Sample	a [nm]	d_{XR} [nm]	u	R_p [%]	R_{wp} [%]	χ^2
A	0.8435(3)	8,1(1)	0.258(2)	7.73	9.92	1.129
B	0.8434(2)	9,3(1)	0.257(1)	6.62	8.60	1.009

a is the lattice parameter, d_{XR}, the mean particle size and u, the oxygen positional parameter. The fitting quality is controlled by R_p, R_{wp} that are reliability factors and χ^2, the goodness of the fit.

As shown in Table 1, the lattice parameter values agree with that presented in the ASTM of 0.844 nm [14]. The oxygen positional parameter is slightly larger than the expected value for an ideal cubic close packed arrangement, equal to 0.25, and in good agreement with recent results [8]. One can remark that if a certain degree of inversion exists in ferrite nanocrystals, it would probably induce some distortion in the oxygen position depending on the divalent metal ionic radius.

Table 2: Atoms position and occupation in the spinel structure.

Atom	Site	Fraction sample (A)	Fraction sample (B)	x	y	z
	A-site					
Zn(A)	8a	0.80(8)	0.78(6)	1/8	1/8	1/8
Fe(A)	8a	0.20(8)	0.22(6)	1/8	1/8	1/8
	B-site					
Zn(B)	16d	0.90(4)	0.89(3)	1/2	1/2	1/2
Fe(B)	16d	0.10(4)	0.11(3)	1/2	1/2	1/2

Positions and fraction of the metal ions in each site. Zn(A) and Fe(A) atoms are located at the tetrahedral A-site; Zn(B) and Fe(B) atoms are at the octahedral B-site.

As it can be seen in Table 2, the occupancies at the tetrahedral A-site and at the octahedral B-site indicate the presence of Fe^{3+} ions at tetrahedral sites in our samples. The value found for the inversion degree, around 0.20, corresponds to the substitution of 1.6 atoms at each kind of the sites. At this stage, one can therefore expect the existence of a non zero magnetic moment associated to a magnetically ordered core in the nanoparticle.

Magnetic and magneto-optical characterization: Let us consider an assemble of independent single-domain grains with a magnetic moment $\mu = \pi m_s d^3/6$; where m_s is the magnetization of the nanoparticle. In the presence of an external field, the liquid matrix with the suspended particles behaves as an ideal superparamagnet and the ferrofluid magnetization is given by the Langevin law [15]: $M = m_s \phi L(\xi)$, $L(\xi) = \coth \xi - \xi^{-1}$, $\xi = \mu_0 \mu H / k_B T$, with ϕ the ferrite volume fraction, k_B the Boltzmann constant ant T the temperature. This equation shows that at $H = 0$ the magnetization is zero. As the field H is turned on, the magnetic moments tend to align in the field direction so that at high fields, M saturates at $m_s \phi$.

The field-induced birefringence behavior [11] is based on the existence of an optical anisotropy axis along the magnetic anisotropy one. Then, in the presence of a field, the magnetic solution exhibits a birefringence $\Delta n = \phi \delta n_0 [1 - 3L(\xi)/\xi]$, $\delta n_0 = C \phi f(\sigma)$ being the optical anisotropy where C depends on the particle refraction index and shape eccentricity. The function $f(\sigma)$ grows from 0 to 1 as its argument $\sigma = E_a / k_B T$ goes from zero to infinity, E_a being the anisotropy energy.

Nevertheless, since the magnetic fluids are always polydisperse, the size distribution must be taken into account in both measurements by considering the volume-weighted superposition of the contributions of all different particle volumes. The particle size distribution is generally well described by a log-normal law. Then, if m_S (magnetization measurements) or δn_0 (birefringence measurements) can be determined by the high field extrapolation, the normalized magnetization or birefringence is reduced to a function of the size distribution parameters, i.e., the characteristic diameter d_0 and its standard deviation s.

A typical normalized magnetization curve is shown in Fig. 3a. Table 3 summarizes the results obtained by fitting the experimental data to the Langevin model. As for both samples, the obtained curves reach the saturation, the high field extrapolation gives the saturation magnetization values m_s. Accordingly, values of m_s =188 ± 5 kA/m and 187 ± 5 kA/m were obtained for samples A and B, respectively. Such high values of the magnetization are an *ultima ratio* in favor of a cation redistribution in the spinel-type nanostructure. Moreover, the values of the size distribution parameter compare well to the crystalline mean size once the X-ray diffraction experiments lead to an average particle diameter given by $d_{XR} = d_0 \exp(2.5s^2)$ [16].

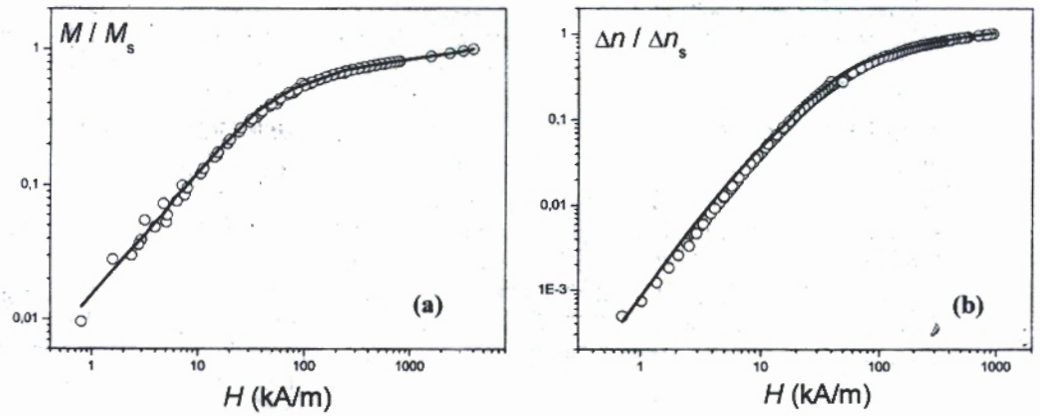

Fig. 3. Reduced magnetization (3a) and reduced birefringence (3b) of sample B as function of the applied magnetic field. The full lines are the best fit obtained by using the Langevin formalism.

Fig. 3b presents a typical normalized birefringence curve. As for the magnetization one, the observed field induced birefringence follows quite well the Langevin model: in particular, the curves readily saturate at high fields, a result that provides the value of the individual particle optical anisotropy δn_0 also listed in Table 3. This optical anisotropy shows a dependence on the grain size, increasing as the diameter of the particle increases, a result that is in good agreement with previous birefringence measurements performed on γ-Fe_2O_3 nanoparticles [11]. Moreover, the values calculated here compare well with the optical anisotropy of 6.3 nm sized (crystalline mean size) $ZnFe_2O_4$ nanoparticles already obtained by using the same experimental technique [15]. The particle sizes deduced from birefringence experiments are higher than those obtained from magnetization ones. This has to be related with the differences between both static experiments since magnetization measurements probes the orientation of the magnetic moment associated to the particle, whereas birefringence technique is more sensitive to the orientation of the anisotropy axis. The latter one is, therefore, relative to the mechanical rotation of the nanograins in solution. As a consequence, superparamagnetic particles with a very small anisotropy energy when compared to the thermal one do not contribute to the birefringence of the colloidal solution. Indeed, when the field is high enough, the Zeeman energy μH of the particle exceeds $k_B T$ and the direction of the magnetic moment of the biggest particles firstly align with H. Then, the orientational effect of H (via internal magnetic anisotropy) on the particle optical axis reaches its maximum, resulting in a saturation of the ferrofluid birefringence. With further increase of H, the magnetization process, which continues with the smallest particles, does not affect Δn any more. In other words, bigger particles contribute more than smaller particles in the birefringence technique.

Table 3: Birefringence and magnetization parameters:

Sample	Magnetization			Birefringence		
	m_s [kA/m]	d_0 [nm]	s	δn_0	d_0 [nm]	s
A	188	6.3	0.32	$2.8\ 10^{-2}$	10.7	0.40
B	187	8.3	0.38	$3.7\ 10^{-2}$	12.6	0.40

m_s is the saturation magnetization and δn_0 the individual optical anisotropy of the particle, both determined from the high field behavior.

Summary

Stoichiometric zinc ferrite nanoparticles have been *bottom up* synthesized and exhibit very peculiar properties. The structural investigation, performed by Rietveld refinement of powder diffractograms, indicates the presence of Fe^{3+} ions at tetrahedral sites of the spinel type nanocrystals and a slight distorsion of oxygen positions. This cation inversion induces the existence of a magnetic moment that is determined at room temperature magnetization measurements realized on diluted colloidal solution. Since such ferrofluids also presents magneto-optical properties, their optical anisotropy was obtained and compares well with that observed for other ferrite magnetic particles.

Acknowledgments

The authors thanks the Brazilian agencies CAPES, CNPq, FAPESP, FAPDF and FINATEC

References

[1] B. Berkovsky: *Magnetic Fluids and Applications Handbook* (Begell, New York, 1996).
[2] X. Battle, A. Labarta: J. Phys. D: Appl. Phys. 35 (2002), p.15.
[3] V. R. K. Murthy, B. Viswanathan: *Ferrite Materials, Science and technology* (Narosa Publishing House, 1990).
[4] B. D. Cullity: *Introduction to Magnetic Materials* (Addison–Wesley, Reading, 1972), p.188.
[5] G. F. Goya, H. R. Rechenberg: J. Magn. Magn. Mater. 196-197 (1999), p.191.
[6] F. K. Lotgering: J. Phys. Chem. Solids 27 (1966), p.139.
[7] W. Schiessl, W. Potzel, H. Karzel, M. Steiner, G.M. Kalvius, A. Martin, M.K. Krause, I. Halevy, J. Gal, W. Schäfer, G. Will, M. Hillberg and R. Wäppling: Phys. Rev. B 53 (1996), p.9143.
[8] F.J. Guaiata, H. Beltrán, E. Cordoncillo, J.B. Carda and P. Escribano: J. Eur. Ceramic 19 (1999), p.363.
[9] H.H. Hamdeh, J.C. Ho, S.A. Oliver, R.J. Willey, G. Oliveri and G.J. Busca: J. Appl. Phys. 81 (1997), p.1851.
[10] J. F. Hochepied, P. Bonville, M. P. Pilen: J. Phys. Chem. B 104 (2000), p.5.
[11] E. Hasmonay, E. Dubois, J. C. Bacri, R. Perzynski, Y. L. Raikher, V. I. Stepanov: Eur. Phys. J. B 5 (1998), p.859.
[12] F. Bernard, J. Lorimier, V. Nivoix, N. Millot, P. Perritat, B. Gillot, J.F. Berar and J.C. Niepce: J. Solid State Chem. Vol. 141 (1998), p.105.
[13] D. Ko, K.R. Poeppelmeier, D.R. Kammler, G.B. Gonzalez, T.O. Mason, D.L. Williamson, D.L. Young and T.J. Coutts: J. Solid State Chem. 163 (2002), p.159.
[14] ASTM n° 22-1012.
[15] J. Depeyrot, G. J. da Silva, C. R. Alves, E. C. Sousa, M. Magalhães, A. M. Figueiredo. Neto: Braz. J. Phys. 31 (2001), p.390.
[16] E. Tronc, D. Bonnin: J. Phys. Lett. 46 (1985), p.L437.